PHYSICS

Photoelectron energy peaks shift against the radiation pressure in strong-field ionization

Kang Lin[1,2]*†, Sebastian Eckart[1]*†, Alexander Hartung[1], Daniel Trabert[1], Kilian Fehre[1], Jonas Rist[1], Lothar Ph. H. Schmidt[1], Markus S. Schöffler[1], Till Jahnke[3], Maksim Kunitski[1], Reinhard Dörner[1]*

The photoelectric effect describes the ejection of an electron upon absorption of one or several photons. The kinetic energy of this electron is determined by the photon energy reduced by the binding energy of the electron and, if strong laser fields are involved, by the ponderomotive potential in addition. It has therefore been widely taken for granted that for atoms and molecules, the photoelectron energy does not depend on the electron's emission direction, but theoretical studies have questioned this since 1990. Here, we provide experimental evidence that the energies of photoelectrons emitted against the light propagation direction are shifted toward higher values, while those electrons that are emitted along the light propagation direction are shifted to lower values. We attribute the energy shift to a nondipole contribution to the ponderomotive potential that is due to the interaction of the moving electrons with the incident photons.

INTRODUCTION

In 1905, the concept of light quanta (termed as photons nowadays) was first proposed by Einstein to explain the photoelectric effect, where a bound electron can only be released to the continuum by absorbing a single photon of an energy that is larger than the ionization potential (*1*). The final kinetic energy of the liberated electron is $E_e = \hbar\omega - I_p$, where ω is the light's frequency, and I_p is the ionization potential of the target. Later, in 1931, Göppert-Mayer (*2*) showed that bound electrons can absorb multiple photons simultaneously such that the electron energy is given by $E_e = n\hbar\omega - I_p$, where n is an integer that is large enough such that the bound electrons can overcome I_p. In 1979, with the advent of pulsed laser techniques, Agostini *et al.* (*3*) found that even free-free transition can happen if the laser intensity is high enough, or—more generally speaking—a bound electron can absorb more photons than needed to overcome I_p. As a result, a series of discrete peaks in the photoelectron's energy domain occur, which are equally spaced by the photon energy of the driving laser field. The phenomenon has been termed above-threshold ionization (ATI) (*4*–*7*) and is shown schematically in Fig. 1.

In case of strong-field ionization, the electric field strength of the driving laser pulse is comparable to the atomic or molecular Coulomb field. Thus, the field-free ionization potential of the atom or molecule is Stark-shifted (*8*), leading to an effective potential $I_p + U_p$ with the ponderomotive energy U_p that is given in atomic units by (*4*)

$$U_p = \frac{F^2}{4\omega^2} \tag{1}$$

Here, F is the peak electric field of the linearly polarized driving field. In principle, the increased effective ionization potential can be compensated for by the gradient force in the focus if the laser pulse is long enough to allow the electron to escape the focus before the laser pulse has faded out. However, for ultrashort laser pulses, with durations of tens of femtoseconds, this is not the case, and thus, the final kinetic energy of photoelectrons produced from ATI process is given by (*4*)

$$E_{\mathrm{ATI},n} = n\hbar\omega - \mathrm{I}_p - U_p \tag{2}$$

Already in 1990, Reiss (*9*) suggested that U_p has to be replaced by an effective ponderomotive potential leading to Eq. 3, which spawned further theoretical work by Böning *et al.*, Jensen *et al.*, Lund and Madsen, and Brennecke and Lein (*10*–*13*)

$$U_p^{\mathrm{eff}}(p_x) = U_p/(1 - p_x/c) \approx (1 + p_x/c)\, U_p \tag{3}$$

This expression for U_p^{eff} includes nondipole (*14*–*21*) contributions to the light-matter interaction, which depend on p_x [see Eq. (21) in (*10*)]. Here, p_x is the electron momentum along the light propagation direction. Accordingly, this prediction suggests that ATI energy peaks do not generally occur as a series of equally spaced peaks, but that the position of the nth ATI peak depends on the electron momentum in the light propagation direction p_x

$$\widetilde{E_{\mathrm{ATI},n}}(p_x) = n\hbar\omega - I_p - (1 + p_x/c)\, U_p \tag{4}$$

Figure 1 illustrates the effect of this nondipole correction on the photoelectron spectrum and highlights that, for certain emission angles, the ATI peaks are not equally spaced anymore as depicted in Fig. 1B and that this nondipole effect is insensitive to the internal structure of the atom or molecule that is ionized. Thus, the difference $\widetilde{E_{\mathrm{ATI},n}}(p_x) - E_{\mathrm{ATI},n}$ increases with the electron momentum in the light propagation direction p_x. The nondipole shift points for all ATI peaks into the direction that is opposite to the radiation pressure. However, the envelope (green line in Fig. 1B) is shifted in the direction that points along the radiation pressure. Note that previously, a seemingly similar backward shift of the envelope for very low electron energies has been observed by Ludwig *et al.* (*14*). The shift that we observe is present for all ATI peaks and even vanishes for very low energy electrons and is thus very different from the one

[1]Institut für Kernphysik, Goethe-Universität, Max-von-Laue-Str. 1, 60438 Frankfurt am Main, Germany. [2]State Key Laboratory of Precision Spectroscopy, East China Normal University, Shanghai 200241, China. [3]European XFEL, 22869 Schenefeld, Germany.
*Corresponding author. Email: lin@atom.uni-frankfurt.de (K.L.); eckart@atom.uni-frankfurt.de (S.E.); doerner@atom.uni-frankfurt.de (R.D.)
†These authors contributed equally to this work.

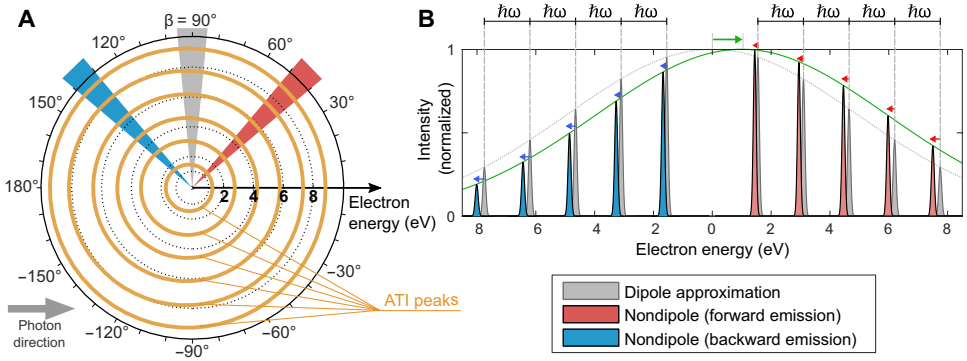

Fig. 1. Illustration of ATI beyond the dipole approximation. (**A**) Within the dipole approximation, a series of concentric circles is formed in energy space, which corresponds to peaks in the energy distribution that are equally spaced by the photon energy. The angle β indicates the electron emission direction with respect to the light propagation direction. For the nondipole case, the concentric circles are deformed (yellow curves; Eq. 4). The deformation is exaggerated for visualization purposes by setting the speed of light to $c = 0.2 \cdot 137$ a.u. = 27.4 a.u. and $U_p = 13.6$ eV = 0.5 a.u. in Eq. 4. The gray dashed lines are circles to guide the eye. (**B**) Energy spectra for the subsets indicated in (A). The colors in (B) correspond to the colors in (A). It is clearly seen that the spacing of the ATI energy peaks, which is often considered to be equal to the photon energy $\hbar\omega$, depends on the electron's emission direction and that the ATI peaks are shifted backward (blue and red arrows). The green line and the green arrow illustrate the shift of the envelope of the ATI peaks (not to scale) that is due to the photon's momentum and that is opposite to the shift of the ATI peaks.

reported by Ludwig *et al.* What is the reason for this backward shift of the ATI peaks? The original dipole approximation–based explanation of ATI is often understood as free-free transitions between the continuum states (*3*). Taking the vector potential into account as in (*13*), this leads to a p_x-dependent ac Stark shift of $(1 + p_x/c)U_p$. For electrons emitted along (against) the light propagation direction, the resonant continuum states are shifted to higher (lower) energies, which lastly results in the backward shift of the ATI rings (*11*–*13*).

An intuitive understanding of the nondipole energy shift can be gained using a simple perspective based on a Doppler-like effect (*10*). To this end, we use that according to Eq. 3, the nondipole corrected ponderomotive potential is $U_p^{\mathrm{eff}}(p_x) \approx (1 + p_x/c)\, U_p$. By analogy with the Doppler shift for a moving object, the frequency of the laser field's time-dependent force acting upon the electron in the laboratory frame is given by $\omega_{\mathrm{eff}} = \omega(1 - p_x/c)$ in atomic units. Thus, this Doppler-like effect would occur also in the absence of the Lorentz force. Inserting ω_{eff} into Eq. 1 results in a predicted energy for the nth ATI peak

$$\widetilde{E^{\mathrm{ATI},n,}_{\mathrm{Doppler}}}(p_x) = n\hbar\omega - I_p - \frac{U_p}{(1 - p_x/c)^2} \approx n\hbar\omega - I_p - (1 + 2p_x/c)\, U_p \quad (5)$$

The expression that is found using the simple Doppler-like effect agrees qualitatively with Eq. 4, but both expressions differ by a factor of 2 in front of p_x/c. The reason for this quantitative difference warrants further research, but recent theoretical findings by Brennecke and Lein (*13*) using circularly polarized light indicate that the nondipole strong field approximation (SFA) model is correct. However, we believe that the very intuitive approach of the Doppler-like model and its capability to make the correct qualitative prediction make it worth to be mentioned.

The origin of ATI peaks in the wave picture

Above, we have used the photon picture and the Stark shift to explain the p_x-dependent shift of the ATI peaks. Alternatively, one can derive Eq. 2 in the wave picture: To this end, we consider an electron bound with $-I_p$. After a part of the electronic wave function has been liberated (and while the laser is still on), this continuum wave packet has an average energy of $E_{\mathrm{elec}} + U_p^{\mathrm{eff,wave}}$, where E_{elec} is the electron's asymptotic energy (at a time when the laser pulse is off), and $U_p^{\mathrm{eff,wave}}$ is the average kinetic energy of the electron due to its quiver motion in the time-dependent electromagnetic field of the laser pulse.

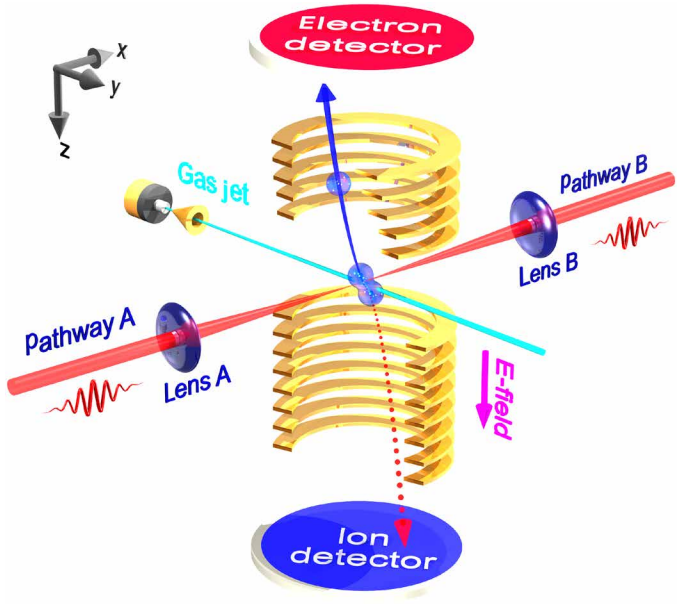

Fig. 2. Schematic diagram of the experimental setup. Two counterpropagating femtosecond laser beams, termed as pathways A and B, respectively, are focused onto the same spot of a supersonic gas jet inside the ultrahigh vacuum chamber of a COLTRIMS reaction microscope that allows for the measurement of electron and ion momenta in coincidence. By toggling between the two counterpropagating pathways of A and B, the systematic error along the light propagation direction can be minimized.

Let us consider two wave packets, which are Ψ_1 and Ψ_2. Ψ_1 is released at time t_1, and Ψ_2 is released at time $t_2 = t_1 + T_{ph}$, where T_{ph}

is the duration of one cycle of the laser field. We assume that both wave packets are identical parts of the same bound state until t_1 and thus $\Psi_1(t_1) = \Psi_2(t_1)$. If we neglect the Coulombic potential, then the time evolution (*22*) from t_1 to t_2 can be expressed via $\Psi_1(t_2) = \Psi_1(t_1) \cdot \exp(i\, T_{\mathrm{ph}}(E_{\mathrm{elec}} + U_p^{\mathrm{eff,wave}})/\hbar)$. The wave packet Ψ_2 is bound until t_2. Therefore, its time evolution is given via $\Psi_2(t_2) = \Psi_2(t_1) \cdot \exp(T_{ph}(-I_p)/\hbar)$. After the time t_2, the relative phase of the two wave packets does not change anymore. Thus, asymptotically, the relative phase of Ψ_1 and Ψ_2 is given by $\phi(E_{\mathrm{elec}}) = T_{\mathrm{ph}}(E_{\mathrm{elec}} + U_p^{\mathrm{eff,wave}})/\hbar - T_{\mathrm{ph}}(-I_p)/\hbar = T_{\mathrm{ph}}(E_{\mathrm{elec}} + U_p^{\mathrm{eff,wave}} + I_p)/\hbar$. This leads to the condition for constructive interference, which is $2\pi = \frac{2\pi}{\omega}(E_{\mathrm{elec}} + U_p^{\mathrm{eff,wave}} + I_p)/\hbar$. This expression can be transformed to $E_{\mathrm{elec}} = \omega\hbar - I_p - U_p^{\mathrm{eff,wave}}$, which equals Eq. 2 for $U_p^{\mathrm{eff,wave}} = U_p^{\mathrm{eff}}$. As expected, the interference of wave packets that are released periodically in time leads to energy quantization. This well-known result illustrates the equivalence of the photon picture and wave picture (*23*, *24*). However, there is another very interesting perspective: If ATI peaks are viewed as an interference phenomenon (*25*), then their position shifts carry information about the phase of the electronic wave function. Thus, the ATI peak positions allow for an interferometric approach to measure $U_p^{\mathrm{eff}}(p_x)$. This approach is independent of predictions as in Eq. 3 or 5.

Unfortunately, it is evident from Eqs. 3 and 4 that the order of magnitude for the expected energy shifts is extremely small for typical experimental conditions in the strong-field regime. For example, a linearly polarized laser pulse with a central wavelength of 800 nm and a peak intensity of 1.0×10^{14} W/cm^2 has a ponderomotive potential of 6.0 eV. For an initial momentum component of $p_x =$ 0.2 atomic units (a.u.), the expected change in ATI peak energy is only $U_p p_x/c \approx 9$ meV.

Experiment with counterpropagating laser beams

The key to successfully resolve such a small energy shift is to minimize systematic errors by using an experimental setup that allows for the ionization of individual atoms or molecules from a gas jet in an experimental geometry where the light propagation direction can be inverted while everything else remains unchanged, as schematically shown in Fig. 2 (*26*, *27*). Briefly, two counterpropagating laser beams are focused onto the same spot in a gas jet to trigger the ionization process. The energy spectra are recorded by a specialized cold target recoil ion momentum spectroscopy (COLTRIMS) setup with extremely high momentum resolution in light propagation direction. With this setup, it is possible to record energy spectra under the exact same experimental conditions except for the inversion of the light propagation direction by using two different laser pathways (see Materials and Methods for details).

RESULTS

Figure 3A displays the measured electron energy spectrum for one of the two laser pathways after restricting the data to a subset of electron emission angles of 9° to 11° with respect to the *y*-*z* plane that is perpendicular to the light propagation direction. Here, the *z* axis is the laser's polarization axis, and the *x* axis is the light propagation direction, as schematically shown in Fig. 2 (see Materials and Methods for more details). This corresponds to values of β from 79°

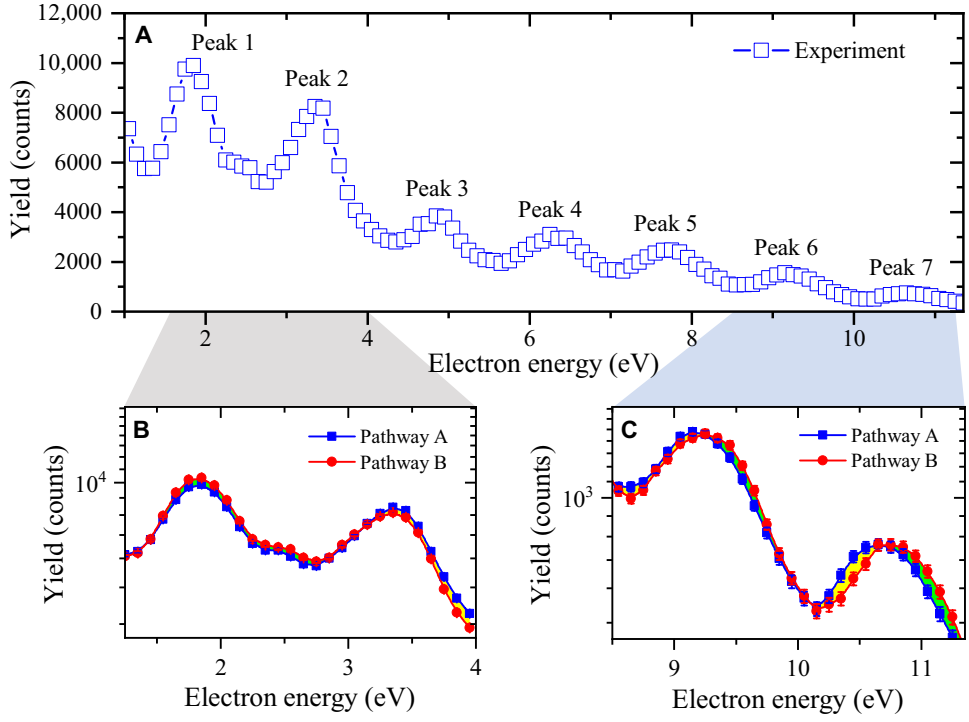

Fig. 3. Measured electron energy spectra. (**A**) Full-range energy spectrum measured for one of the two counterpropagating laser pathways. (**B** and **C**) Subsets of (A), where the spectra measured from the two opposite pathways are overlapped. Only the subsets of electrons emitted under an angle of about 10° with respect to the plane perpendicular to the light propagation direction are considered. The error bars show statistical errors. For (A) and (B), the error bars are smaller than the data points.

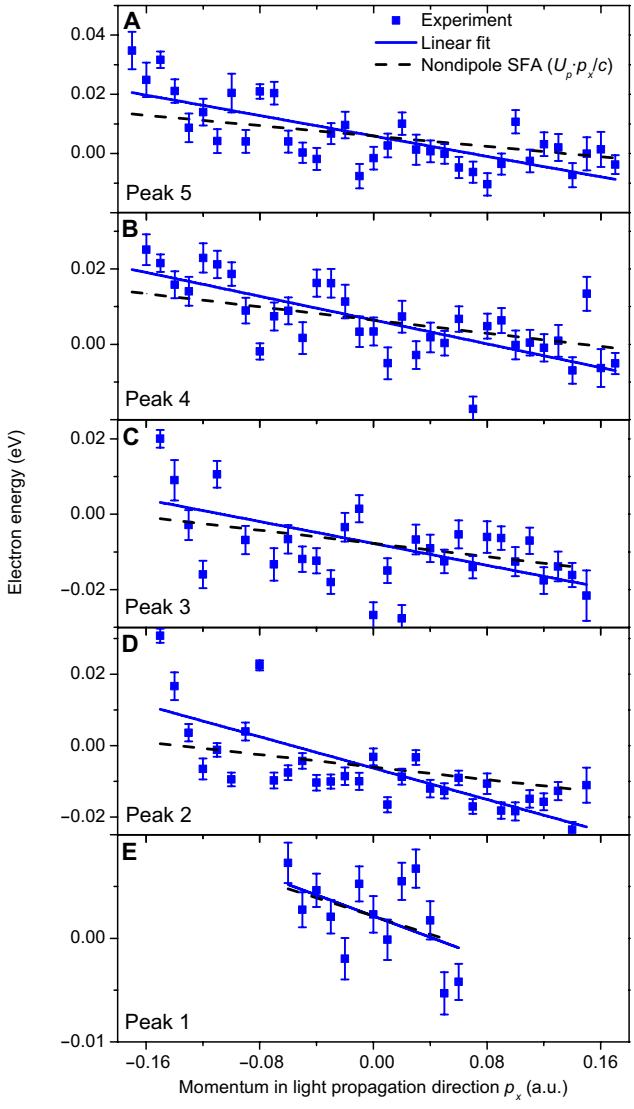

Fig. 4. Measured nondipole electron energy shift. (**A** to **E**) Shift of the peak position of the ATI peaks as a function of the momentum in light propagation direction p_x for the first five ATI peaks (see Fig. 3A). The data points are determined by fitting Gaussians to the data and taking the average of the two counterpropagating laser pathways as reference. The expectations from nondipole SFA are shown in black dashed lines. The error bars show fitting errors.

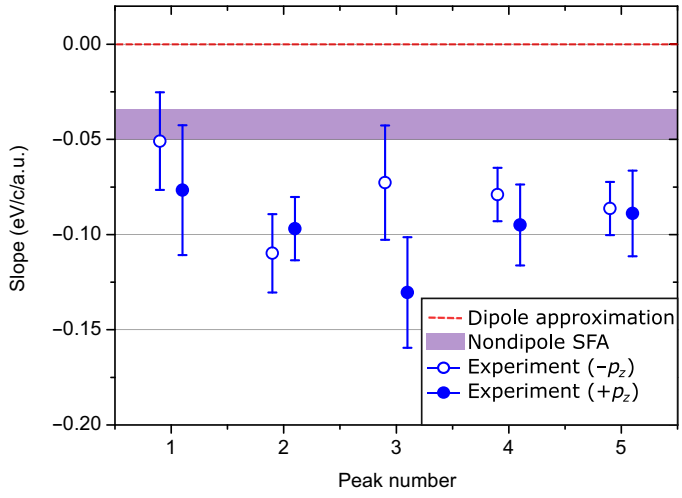

Fig. 5. Comparison of experimentally obtained nondipole energy shifts and the theoretical prediction. The slopes of the linear fits from Fig. 4 are shown in units of electron volts/c per a.u. (blue open circles) where only negative p_z values were used (p_z is the momentum along the polarization direction). c is the speed of light. As a cross-check, the filled circles show the same as the open circles but use the data that have positive momenta in polarization direction (p_z). The red dashed line indicates the slope within the dipole approximation, which is zero. The purple shaded area indicates the expectations from the nondipole SFA (Eq. 4) by considering an uncertainty of ±20% for the intensity calibration. The error bars show the statistical error.

to 81° and from 99° to 101° in Fig. 1A. This angular restriction results from a compromise between high statistics for small values of $|p_x|$ and an increased nondipole effect for large values of $|p_x|$. As expected, the two energy spectra collected from the two counterpropagating laser beams are almost identical since the maximum shift is expected to be on the order of only 18 meV for $p_x = \pm 0.2$ a.u. For the low-energy peaks in Fig. 3B, the peak positions are almost exactly congruent for the two laser beam pathways. This is expected because for electrons emitted along a fixed angle, low electron energies correspond to small values of p_x. Notably, for the high-energy part of the spectrum, as shown in Fig. 3C, a clear shift of the peak positions is observed. In addition, the magnitude of the difference, which is on the order of tens of millielectron volts, agrees with the expectation.

For a full quantitative analysis, we plot the extracted nondipole energy shift for the first five ATI peaks as a function of photoelectron momentum along the light propagation direction p_x in Fig. 4. The position of each ATI peak is obtained by Gaussian fits. The systematic error is minimized by taking the average of the two peak energy values, which are obtained from the two incident beams propagating in opposite directions, as reference. Figure 4 shows the case where the light propagation direction points to the positive p_x direction. The decrease in the ATI peak energy as a function of p_x is clearly visible. Thus, our experimental results confirm the prediction that the ATI peak energies for electron emission directions that are parallel to the light propagation direction are lower than for electrons that are emitted antiparallel to the light propagation direction. The shift is thus indeed opposite to what one might have naively expected from the direction of the radiation pressure.

DISCUSSION

Figure 5 summarizes the experimental results by depicting the slopes of the linear fits from Fig. 4 for each energy peak separately (see open circles in Fig. 5). To compare our experimental findings, we show the results together with the prediction from the nondipole SFA (Eq. 4) (*10*–*12*). For the SFA model, we use a ponderomotive potential that corresponds to the laser intensity used in the experiment (taking the uncertainty of the intensity calibration into account). It is unexpected that our measurement shows a substantially higher p_x dependence compared to the result from the nondipole SFA.

To further cross-check our experimental findings, we make use of the symmetry of linearly polarized light. For Fig. 4, we only analyzed half of the electron momentum distribution that has negative values for p_z (momentum in the polarization direction). The filled circles in Fig. 5 are obtained in full analogy to the open circles, but

for these data points, the other half of the electron momentum distribution is used, which has positive p_z.

As expected, the filled and open circles show consistent results and indicate that the systematic errors are comparable to the statistical errors. Possible reasons for the experimentally observed enhancement of the energy shift compared to the nondipole SFA model are recollision dynamics (*14*, *28*) and Coulomb interaction during and after tunneling (*29*), which are not included in the nondipole SFA model but could be relevant (especially for linearly polarized light). Furthermore, the nondipole SFA model was developed for atoms. In our experiment, we study H_2 that is expected to show very similar tunneling dynamics in comparison with atoms (*30*). However, recollision dynamics are sensitive to the excited states of the ion (*31*), which might be a reason for the experimentally observed enhancement of the energy shift compared to the nondipole SFA. As outlined above, ATI peaks can be explained by intercycle interference (*24*). Consequently, different types of interference could contribute to the observed energy shift. For instance, it is conceivable that the interplay of Coulomb interaction with subcycle interference (*32*) or holography (*33*–*35*) is affected by nondipole corrections, which could modulate (*36*) the ATI peak positions. This is in line with the findings of Brennecke and Lein (*37*) who showed that a rigorous treatment of nondipole effects is necessary to model interference using semiclassical models. Moreover, the liberated electron stems from a σ orbital. Thus, the initial electronic state cannot have angular momentum. Furthermore, the symmetry of linearly polarized light implies that a potential fingerprint of a nonvanishing magnetic quantum number would not manifest as rotation as in (*38*). Future theoretical studies might also investigate the role of properties of the initial electronic state (as, e.g., the electron's magnetic quantum number) on the ATI peak positions.

In our previous work (*27*), another electric nondipole effect was reported for strong-field ionization driven by a circularly polarized laser pulse. In that work, it was found that the most probable photoelectron's momentum component in the polarization plane varies as a function of momentum component in the light propagation direction. It is important to note that in (*27*), the envelope shifts (see Fig. 1B), and in our current work, we see a shift of the ATI peak positions. Furthermore, the shift in our current work leads to a decrease in energy as a function of p_x, and in (*27*), the shift leads to an increase in the energy of the peak of the envelope as a function of p_x. Thus, the shift in our current work points into the opposite direction compared to the shift in (*27*) and is related to an independent observable. As the observable in the current work, the ATI peak position is modified by nondipole effects that alter the phase of the electronic wave function in momentum space representation and thereby shift the ATI peak positions, which are an interference phenomenon. The shift in (*27*) is not related to inference and can be explained by classical acceleration. Nevertheless, both shifts are closely related to the ponderomotive potential as it has been shown theoretically in (*13*).

We show that ATI peaks occurring in strong-field ionization are only equally spaced in energy for electrons that are emitted perfectly at the right angle to the light propagation direction, qualitatively confirming a theoretic prediction from 1990 (*9*). For all other emission directions, the spatiotemporal evolution of the electric field results in ATI peaks that are not equally spaced in energy. Moreover, we have observed that the nondipole energy shift depends on the photoelectron momentum in light propagation direction (p_x). The ATI peak energies decrease (increase) compared to the expectations from the dipole approximation for electrons that are emitted in the forward (backward) hemisphere. The shifts of the ATI peaks as a function of the momentum in the light propagation direction (p_x) can be described as a p_x-dependent ac Stark shift (*13*). Our results show that the shifts of the ATI peak energies have a direction that is opposite to the direction of the shift that is due to the photon momentum (i.e., light pressure) (*27*). We expect that similar corrections should lead to a broadening of the photon's energy spectra for high harmonic generation.

MATERIALS AND METHODS

Experimental design

The two counterpropagating laser beams were generated from a Ti:Sapphire laser system (Coherent Legend Elite). The output of the laser system (25 fs, 800 nm, 10 kHz) is split into two pathways using a dielectric beam splitter, termed as pathways A and B, respectively. The intensity and polarization of each laser pathway can be adjusted independently. Eventually, the two linearly polarized laser beams are focused into the vacuum chamber of a COLTRIMS reaction microscope (*39*) from two opposite sides using two independent lenses (f = 25 cm) onto the same spot inside a supersonic gas jet of H_2 molecules. For both laser pulses, the polarization axis is aligned along the z direction. Two motorized shutters placed in the two beam pathways are used to toggle between both pathways every 3 min to minimize systematic errors. The peak intensity in the laser focus is found to be 1.0×10^{14}W/cm^2 with an uncertainty of ±20%. For laser intensity calibration, the ratio between double and single ionization yield of xenon atom is recorded and compared to values given in (*40*).

A static electric field of 29.8 V/cm was applied to guide the electrons and ions created from single ionization of H_2 molecules to two time- and position-sensitive detectors at opposite ends of the spectrometer (*41*). The acceleration lengths of the field region for electrons and ions are 15 and 58 cm, both of which are followed by a field-free drift region of 30 and 108 cm, respectively. The electron (ion) detector is composed of a three-layer (two-layer) stack of multichannel plates followed by a three-layer delay-line anode. The three-dimensional momenta of the electrons and ions were retrieved coincidently from the times of flight and positions of impact. The z direction is the time-of-flight direction of the COLTRIMS reaction microscope. The single-event momentum resolution of our COLTRIMS reaction microscope for the detection of a single electron is 0.003 a.u. in p_x and p_y directions and 0.03 a.u. in p_z direction.

REFERENCES AND NOTES

1. A. Einstein, Über einen die Erzeugung und Verwandlung des Lichtes betreffenden heuristischen Gesichtspunkt. *Ann. Phys.* **322**, 132–148 (1905).
2. M. Göppert-Mayer, Über Elementarakte mit zwei Quantensprüngen. *Ann. Phys.* **401**, 273–294 (1931).
3. P. Agostini, F. Fabre, G. Mainfray, G. Petite, N. K. Rahman, Free-free transitions following six-photon ionization of xenon atoms. *Phys. Rev. Lett.* **42**, 1127–1130 (1979).
4. R. R. Freeman, P. H. Bucksbaum, H. Milchberg, S. Darack, D. Schumacher, M. E. Geusic, Above-threshold ionization with subpicosecond laser pulses. *Phys. Rev. Lett.* **59**, 1092–1095 (1987).
5. L. V. Keldysh, Ionization in the field of a strong electromagnetic wave. *J. Exp. Theor. Phys.* **20**, 1307–1314 (1965).
6. A. M. Perelomov, V. S. Popov, M. V. Terent'ev, Ionization of atoms in an alternating electric field. *Sov. J. Exp. Theor. Phys.* **23**, 924 (1966).

7. D. B. Milošević, G. G. Paulus, D. Bauer, W. Becker, Above-threshold ionization by few-cycle pulses. *J. Phys. B.* **39**, R203–R262 (2006).
8. R. Shakeshaft, R. M. Potvliege, M. Dörr, W. E. Cooke, Multiphoton processes in an intense laser field. IV. The static-field limit. *Phys. Rev. A.* **42**, 1656–1668 (1990).
9. H. R. Reiss, Relativistic strong-field photoionization. *J. Opt. Soc. Am. B.* **7**, 574–586 (1990).
10. B. Böning, W. Paufler, S. Fritzsche, Nondipole strong-field approximation for spatially structured laser fields. *Phys. Rev. A* **99**, 053404 (2019).
11. S. V. B. Jensen, M. M. Lund, L. B. Madsen, Nondipole strong-field-approximation Hamiltonian. *Phys. Rev. A* **101**, 043408 (2020).
12. M. M. Lund, L. B. Madsen, Nondipole photoelectron momentum shifts in strong-field ionization with mid-infrared laser pulses of long duration. *J. Phys. B.* **54**, 165602 (2021).
13. S. Brennecke, M. Lein, Nondipole modification of the ac Stark effect in above-threshold ionization. *Phys. Rev. A* **104**, L021104 (2021).
14. A. Ludwig, J. Maurer, B. W. Mayer, C. R. Phillips, L. Gallmann, U. Keller, Breakdown of the dipole approximation in strong-field ionization. *Phys. Rev. Lett.* **113**, 243001 (2014).
15. I. A. Ivanov, J. Dubau, K. T. Kim, Nondipole effects in strong-field ionization. *Phys. Rev. A* **94**, 033405 (2016).
16. J. P. Connerade, V. K. Dolmatov, S. T. Manson, Controlled strong non-dipole effects in photoionization of confined atoms. *J. Phys. B.* **33**, L275–L282 (2000).
17. S. Chelkowski, A. D. Bandrauk, P. B. Corkum, Photon-momentum transfer in photoionization: From few photons to many. *Phys. Rev. A* **95**, 053402 (2017).
18. S. Chelkowski, A. D. Bandrauk, P. B. Corkum, Photon momentum sharing between an electron and an ion in photoionization: From one-photon (photoelectric effect) to multiphoton absorption. *Phys. Rev. Lett.* **113**, 263005 (2014).
19. S. Brennecke, M. Lein, High-order above-threshold ionization beyond the electric dipole approximation: Dependence on the atomic and molecular structure. *Phys. Rev. A* **98**, 063414 (2018).
20. J. Daněk, M. Klaiber, K. Z. Hatsagortsyan, C. H. Keitel, B. Willenberg, J. Maurer, B. W. Mayer, C. R. Phillips, L. Gallmann, U. Keller, Interplay between Coulomb-focusing and non-dipole effects in strong-field ionization with elliptical polarization. *J. Phys. B.* **51**, 114001 (2018).
21. C. T. L. Smeenk, L. Arissian, B. Zhou, A. Mysyrowicz, D. M. Villeneuve, A. Staudte, P. B. Corkum, Partitioning of the linear photon momentum in multiphoton ionization. *Phys. Rev. Lett.* **106**, 193002 (2011).
22. C. S. Adams, M. Sigel, J. Mlynek, Atom optics. *Phys. Rep.* **240**, 143–210 (1994).
23. P. Salières, B. Carré, F. Le Déroff, L. Grasbon, G. G. Paulus, H. Walther, R. Kopold, W. Becker, D. B. Milošević, A. Sanpera, M. Lewenstein, Feynman's path-integral approach for intense-laser–atom interactions. *Science* **292**, 902–905 (2001).
24. D. G. Arbó, E. Persson, J. Burgdörfer, Time double-slit interferences in strong-field tunneling ionization. *Phys. Rev. A* **74**, 63407 (2006).
25. F. Lindner, M. G. Schätzel, H. Walther, A. Baltuška, E. Goulielmakis, F. Krausz, D. B. Milošević, D. Bauer, W. Becker, G. G. Paulus, Attosecond double-slit experiment. *Phys. Rev. Lett.* **95**, 040401 (2005).
26. A. Hartung, S. Eckart, S. Brennecke, J. Rist, D. Trabert, K. Fehre, M. Richter, H. Sann, S. Zeller, K. Henrichs, G. Kastirke, J. Hoehl, A. Kalinin, M. S. Schöffler, T. Jahnke, L. P. H. Schmidt, M. Lein, M. Kunitski, R. Dörner, Magnetic fields alter strong-field ionization. *Nat. Phys.* **15**, 1222–1226 (2019).
27. A. Hartung, S. Brennecke, K. Lin, D. Trabert, K. Fehre, J. Rist, M. S. Schöffler, T. Jahnke, L. P. H. Schmidt, M. Kunitski, M. Lein, R. Dörner, S. Eckart, Electric nondipole effect in strong-field ionization. *Phys. Rev. Lett.* **126**, 053202 (2021).
28. T. Keil, D. Bauer, Coulomb-corrected strong-field quantum trajectories beyond dipole approximation. *J. Phys. B.* **50**, 194002 (2017).
29. T.-M. Yan, D. Bauer, Sub-barrier Coulomb effects on the interference pattern in tunneling-ionization photoelectron spectra. *Phys. Rev. A* **86**, 053403 (2012).
30. M. Liu, Y. Liu, Application of the partial-Fourier-transform approach for tunnel ionization of molecules. *Phys. Rev. A* **93**, 043426 (2016).
31. J. Wassaf, V. Véniard, R. Taïeb, A. Maquet, Roles of resonances and recollisions in strong-field atomic phenomena: Above-threshold ionization. *Phys. Rev. A* **67**, 053405 (2003).
32. S. Eckart, M. Kunitski, I. Ivanov, M. Richter, K. Fehre, A. Hartung, J. Rist, K. Henrichs, D. Trabert, N. Schlott, L. P. H. Schmidt, T. Jahnke, M. S. Schöffler, A. Kheifets, R. Dörner, Subcycle interference upon tunnel ionization by counter-rotating two-color fields. *Phys. Rev. A* **97**, 041402 (2018).
33. M. Meckel, D. Comtois, D. Zeidler, A. Staudte, D. Pavičić, H. C. Bandulet, H. Pépin, J. C. Kieffer, R. Dörner, D. M. Villeneuve, P. B. Corkum, Laser-induced electron tunneling and diffraction. *Science* **320**, 1478–1482 (2008).
34. C. F. de Morisson Faria, A. S. Maxwell, It is all about phases: Ultrafast holographic photoelectron imaging. *Reports Prog. Phys.* **83**, 034401 (2020).
35. Y. Huismans, A. Rouzée, A. Gijsbertsen, J. H. Jungmann, A. S. Smolkowska, P. S. W. M. Logman, F. Lépine, C. Cauchy, S. Zamith, T. Marchenko, J. M. Bakker, G. Berden, B. Redlich, A. F. G. van der Meer, H. G. Muller, W. Vermin, K. J. Schafer, M. Spanner, M. Y. Ivanov, O. Smirnova, D. Bauer, S. V. Popruzhenko, M. J. J. Vrakking, Time-resolved holography with photoelectrons. *Science* **331**, 61–64 (2011).
36. S. Eckart, D. Trabert, K. Fehre, A. Geyer, J. Rist, K. Lin, F. Trinter, L. P. H. Schmidt, M. S. Schöffler, T. Jahnke, M. Kunitski, R. Dörner, Sideband modulation by subcycle interference. *Phys. Rev. A* **102**, 043115 (2020).
37. S. Brennecke, M. Lein, Strong-field photoelectron holography beyond the electric dipole approximation: A semiclassical analysis. *Phys. Rev. A* **100**, 023413 (2019).
38. K. Liu, H. Ni, K. Renziehausen, J.-M. Rost, I. Barth, Deformation of atomic p± orbitals in strong elliptically polarized laser fields: Ionization time drifts and spatial photoelectron separation. *Phys. Rev. Lett.* **121**, 203201 (2018).
39. J. Ullrich, R. Moshammer, A. Dorn, R. Dörner, L. P. H. Schmidt, H. Schmidt-Böcking, Recoil-ion and electron momentum spectroscopy: Reaction-microscopes. *Reports Prog. Phys.* **66**, 1463–1545 (2003).
40. J. L. Chaloupka, J. Rudati, R. Lafon, P. Agostini, K. C. Kulander, L. F. DiMauro, Observation of a transition in the dynamics of strong-field double ionization. *Phys. Rev. Lett.* **90**, 033002 (2003).
41. O. Jagutzki, A. Cerezo, A. Czasch, R. Dörner, M. Hattas, M. Huang, V. Mergel, U. Spillmann, K. Ullmann-Pfleger, T. Weber, H. Schmidt-Böcking, G. D. W. Smith, Multiple hit readout of a microchannel plate detector with a three-layer delay-line anode. *IEEE Trans. Nucl. Sci.* **49**, 2477–2483 (2002).

Acknowledgments: We acknowledge helpful discussion with S. Brennecke, M. Lein, and L. B. Madsen. **Funding:** The experimental work was supported by the DFG (German Research Foundation). K.L. acknowledges support by the Alexander von Humboldt Foundation and thanks W. Zhang for sharing the graphic ingredients. S.E. acknowledges funding of the DFG through Priority Programme SPP 1840 QUTIF. A.H. and K.F. acknowledge support by the German Academic Scholarship Foundation. **Author contributions:** K.L., S.E., A.H., D.T., K.F., J.R., L.P.H.S., M.S.S., T.J., M.K., and R.D. contributed to the experiment. K.L., S.E., and R.D. performed the data analysis. All authors contributed to the manuscript. **Competing interests:** The authors declare that they have no competing interests. **Data and materials availability:** All data needed to evaluate the conclusions in the paper are present in the paper and/or the Supplementary Materials. The data that support the findings of this study are available on Zenodo https://doi.org/10.5281/zenodo.5916791.

Submitted 21 December 2021
Accepted 2 February 2022
Published 25 March 2022
10.1126/sciadv.abn7386